Multiscale Contour Extraction Using a Level Set Method in Optical Satellite Images

Qizhi Xu, Bo Li, Zhaofeng He, and Chao Ma

***Abstract*—This letter presents a novel coarse-to-fine level set method for contour extraction in optical satellite images. To distinguish objects from a background, the undecimated wavelet transform is firstly adopted to extract image features, and a homogeneity metric is defined to measure the variation of the features inside and outside contours. In addition, the weight distribution ratio is proposed to adaptively tune the relative weight of the features. Based on the homogeneity metric and the weight distribution ratio, a novel energy functional is developed to model a contour extraction problem, and in order to reduce the computation burden, a coarse-to-fine scheme is applied to progressively extract contours in finer scale, during which a contour position constraint is introduced to limit contours evolving in a small space around the candidate contours extracted in coarser scale. Extensive experiments have been carried out on optical satellite images to validate the proposed method.**

***Index Terms*—Contour extraction, homogeneity metric, level set methods, undecimated wavelet transform (UWT).**

I. Introduction

Contour extraction is an important and challenging image segmentation problem in computer vision. Object contours are free of texture edges and are important features for shape-based object recognition. The aim of this letter is to find the complete 2-D boundaries of the salient objects in optical satellite images via a level set method. It is a hard problem that remains largely unsolved since the mid-1960s [1]. In addition, with the increasing availability of high-resolution satellites and airborne sensors, satellite images capture more details and complex structures of an observed scene and thus poses new challenges for contour extraction. Here, we mainly focus on two challenges.

1) The first is feature extraction. Contour extraction methods are largely dependent on the features of the highly discriminative ability to distinguish objects from a background. However, traditional features are generally of high dimensionality and computationally expensive. Furthermore, it is difficult to measure the relative weight of different features.
2) Then, the second one is the computation burden. The size of objects becomes larger and larger due to finer resolution of modern sensors, but most contour extraction methods are time consuming as size increases. Hence, reducing computational cost is a key issue for high-resolution optical satellite images.

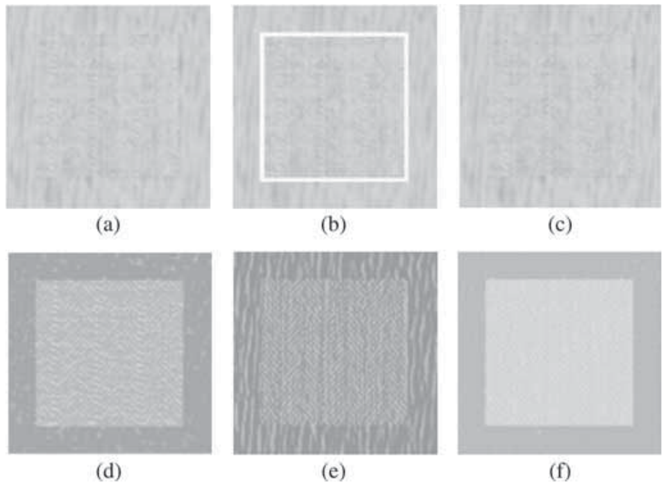

Fig. 1. Differences of the discriminative ability between wavelet coefficient components. (a) Original image. (b) Hand-labeled object. (c)–(f) Four wavelet coefficient components. It is easy to distinguish the object from the background in (d)–(f), whereas it is hard in (c).

Many level set methods [2]–[8] have been proposed to solve the contour extraction problem, but they come up against difficulties when dealing with the aforementioned challenges. Most level set methods [2]–[5] mainly use intensity differences between objects and the background to extract object contours, and these methods [3]–[5] are mainly based on the probability distribution of intensity feature values for the sake of robustness to noise. However, as being pointed out in [2], there are objects that cannot be detected using only intensity features [see Fig. 1(a)]. This situation is even more common in optical satellite images. To overcome this problem, tensor features, which comprehensively represent the texture and intensity information of images, were introduced into the level set methods [6], [7]. Tensor-based methods provide a significant improvement for texture-rich images. For example, the method in [6] dynamically tunes the relative weight of tensor features and consequently outperforms other methods in real applications. However, despite the dimension reduction of tensor features, the computation burden of these methods is also greatly increased. In some cases, the dimension reduction can lose significant information of tensor features, thus resulting in failures of contour extraction. Unlike the aforementioned methods, a multiscale stochastic level set method was developed in [8] to find a global optimization of image segmentation. This method improves the robustness of the methods [2]–[5] and works well on intensity-homogeneous images.

Manuscript received September 1, 2010; revised January 24, 2011 and February 15, 2011; accepted March 8, 2011. Date of publication April 29, 2011; date of current version August 26, 2011. This work was supported in part by the National Basic Research Program of China under Grant 2010CB327900 and in part by the Defense Industrial Technology Development Program of China under Grant BXX2011XXX8.

The authors are with the State Key Laboratory of Virtual Reality Technologies and Systems and the Beijing Key Laboratory of Digital Media, School of Computer Science and Engineering, Beihang University, Beijing 100191, China (e-mail: boli@buaa.edu.cn).

Digital Object Identifier 10.1109/LGRS.2011.2128855

In this letter, we propose a level-set-based multiscale method that exploits weighted wavelet features to extract the contours of salient objects. The method is evaluated on optical satellite images, and a quantitative comparison of the proposed method with the methods in [6] and [8] is provided. The main contributions of this letter are as follows. First, the weighted wavelet features are introduced into the level set method to distinguish objects from the background. Second, based on the wavelet features, a novel energy functional is proposed to model the contour extraction problem. Finally, a coarse-to-fine scheme is developed to reduce computational cost.

The remainder of this letter is organized as follows. In Section II, a feature extraction method is presented. A contour extraction method is described in Section III, and the numerical solution of the proposed method is described in Section IV. Extensive experiments on the optical satellite image database are presented in Section V, whereas the conclusions are drawn in Section VI.

II. Feature Extraction

A. Wavelet Feature Extraction

Here, we present the wavelet feature extraction method implemented by the undecimated wavelet transform (UWT) [8]. The reason for choosing the UWT is that the UWT is shift invariant and produces subbands of the same size as the input image. Using the Haar filter banks $g = [0.5,\ 0.5]$ and $h = [0.5,\ -0.5]$, image I is decomposed into the four subbands w^1, w^2, w^3, and w^4 by the UWT as follows:

$$\begin{aligned} w^1(x,\ y) &= (gg * I)(x,\ y) \qquad & w^2(x,\ y) &= (gh * I)(x,\ y) \\ w^3(x,\ y) &= (hg * I)(x,\ y) \qquad & w^4(x,\ y) &= (hh * I)(x,\ y) \end{aligned} \quad (1)$$

where $gh * I$ is the convolution of image I, first along the columns by g and, then, along the rows by h. Each wavelet subband $w^i (i = 1,\ 2,\ 3,\ 4)$ has the same size as image I.

Let $d^1 = |w^1|$, $d^2 = |w^2|$, $d^3 = |w^3|$, and $d^4 = |w^4|$. d^1 represents the intensity information of image I. d^2, d^3, and d^4 represent the horizontal-, vertical-, and diagonal-direction texture information of image I. Because most of the image energy is concentrated in d^1, the values of $d^i (i = 1,\ 2,\ 3,\ 4)$ are rescaled to a [0,, 1] interval to balance the image energy of d^i.

B. Adaptive Weighting Approach for the Wavelet Feature

Due to the orientation selectivity and bandpass filtering of the wavelet transform, the discriminative ability of the feature components d^i to distinguish objects from the background is significantly different. It is therefore necessary to assign different weights to the feature components according to the discriminative abilities. As shown in Fig. 1, it is clear that the object can be easily detected in components d^2, d^3, and d^4, so that we should assign higher weights to them. To the best of our knowledge, there is no exisiting reference in the literature about using the discriminative abilities to assign feature weights so far. Thus, the weight distribution ratio is proposed to deal with this problem. We argue that the discriminative ability of d^i should positively relate to the homogeneous difference between the areas inside and outside the contours.

Before defining the discriminative ability of d^i, we first introduce a so-called homogeneity metric for d^i. For a given component d^i, Ω_0 denotes the whole region of d^i. The closed curves c, which are introduced by the level set method, divide region Ω_0 into two parts: Ω_1 is the region inside c, and Ω_2 is the region outside c. The homogeneity metric of d^i in region $\Omega_k (k = 0,\ 1,\ 2)$ is defined by

$$E(d^i,\ \Omega_k) = \int_{\Omega_k} \left(d^i(x,\ y) - \bar{d}^i_k\right)^2 dxdy \quad (2)$$

where $\bar{d}^i_k$ is the mean value of d^i over region Ω_k. It is obvious that the homogeneity metric $E(d^i,\ \Omega_k)$ (or $E_{i,\,k}$ for short) is inversely related to the homogeneity of d^i over region Ω_k.

Based on the homogeneity metric aforementioned, the discriminative ability of d^i can be measured by

$$\eta(d^i,\ c) = \frac{E_{i,\,0} + \epsilon_0}{E_{i,\,1} + E_{i,\,2} + \epsilon_0} \quad (3)$$

where ϵ_0 is a small positive quantity to avoid the denominator vanishing. The weight distribution ratio of d^i is then defined as follows:

$$\xi(d^i,\ c) = \frac{\eta(d^i,\ c)}{\sum_{j=1}^{4} \eta(d^j,\ c)}. \quad (4)$$

For the sake of simplicity, $\xi(d^i,\ c)$ and $\eta(d^i,\ c)$ are denoted by $\xi_{i,\,c}$ and $\eta_{i,\,c}$, respectively. Since the discriminative ability term $\eta_{i,\,c}$ is dependent on curve c, $\xi_{i,\,c}$ is therefore adaptively calculated in the level set evolution.

$\xi_{i,\,c}$ is a reasonable metric for assigning different weights for d^i. For example, let c denote object contours. If $E_{i,\,0} \approx E_{i,\,1} + E_{i,\,2}$, then it is hard to distinguish the objects from the background in d^i, and $\xi_{i,\,c}$ is small. If $E_{i,\,0} \gg E_{i,\,1} + E_{i,\,2}$, then the objects can be easily distinguished from the background in d^i, and $\xi_{i,\,c}$ is large. Based on the above analysis, the weighted feature components are expressed by

$$\left\{ (\xi_{i,\,c})^{\frac{1}{2}} d^i \mid i = 1,\ 2,\ 3,\ 4 \right\}. \quad (5)$$

III. Model Description

We use a four-point average downsampling scheme, which reduces the resolution one level at a time, to create the low-resolution images for multiscale contour extraction. In what follows, S_1 denotes the image scale without downsampling, and S_N denotes the image scale performing downsampling by $N - 1$ times. In our method, the candidate contours are firstly extracted in scale S_N (see Section III-A), and then, the contours are progressively refined from scales S_{N-1} to S_1 (see Section III-B).

A. Model for Coarse-Scale Contour Extraction

The coarse-scale model is the minimization of an energy functional, which is the summation of the weighted homogeneity metrics of the four components in regions Ω_1 and Ω_2. For an image containing M objects, the contours $\hat{c}$ of the objects should satisfy the following contour condition: There exists at least one feature component d^j that satisfies $E_{j,\,0} \gg 0$ and

$E_{j,1} + E_{j,2} \approx 0$. Then, the object contours $\hat{c}$ can be expressed by the minimization of an energy functional as follows:

$$\hat{c} = \arg\min_c \sum_{i=1}^{4} \xi_{i,c}(E_{i,1} + E_{i,2}). \tag{6}$$

The basic idea here is as follows: If d^i satisfies the contour condition, then $E_{i,1} + E_{i,2} \approx 0$, such that $\xi_{i,\hat{c}}(E_{i,1} + E_{i,2}) \approx 0$, and if d^i does not satisfy the contour condition, then $\xi_{i,\hat{c}} \approx 0$, so that $\xi_{i,\hat{c}}(E_{i,1} + E_{i,2}) \approx 0$. Therefore, the object contours can be modeled as the minimization of the above energy functional.

Let $\phi(x, y)$ (ϕ or $\phi_{x,y}$ for short) denote the level set function, then $\phi > 0$ and $\phi < 0$ represent regions Ω_1 and Ω_2, respectively, and $H(x)$ (H_x for short) denotes the Heaviside function, which satisfies $H_x = 1$ for $x \geq 0$ and $H_x = 0$ for $x < 0$. In addition, we add the curve length metric term to the minimization model. With the aforementioned definitions, the level set formulation of the minimization model is given by

$$F_N(c) = \mu \int_{\Omega_0} |\nabla H_\phi| dxdy + \sum_{i=1}^{4} \xi_{i,c} \int_{\Omega_0} \left(d^i - \bar{d}_1^i\right)^2 H_\phi \, dxdy + \sum_{i=1}^{4} \xi_{i,c} \int_{\Omega_0} \left(d^i - \bar{d}_2^i\right)^2 (1 - H_\phi) dxdy \tag{7}$$

where $\int_{\Omega_0} |\nabla H_\phi| dxdy$ is the curve length metric, and μ is the weight of this metric. Using this model, we can extract the candidate contours in the coarsest scale S_N with relatively low computational cost, which paves the way for fine-scale contour extraction.

B. Model for Fine-Scale Contour Extraction

The contour extraction model for scale $S_\alpha (1 \leq \alpha < N)$ is the minimization of an energy functional as well. The only difference is that a contour position constraint is introduced into this model to reduce the contour evolution space to a small region, which surrounds the candidate contours extracted in scale $S_{\alpha+1}$. The contour position constraint is measured by the distance to the candidate contours. First, the candidate contours of scale $S_{\alpha+1}$ in location (i, j) are mapped to locations $(2i - 1, 2j - 1)$, $(2i - 1, 2j)$, $(2i, 2j - 1)$, and $(2i, 2j)$ in scale S_α. In this way, we get the two-pixel width curve γ_α. We assume that the actual contour position is inversely related to its distance to curve γ_α. Therefore, the contour position constraint can be expressed by

$$R_\alpha(x, y) = \exp\left(-\frac{d(x, y, \gamma_\alpha) - 1}{2}\right) \tag{8}$$

where $d(x, y, \gamma_\alpha)$ denotes the distance of position (x, y) to curve γ_α. Similar to the coarse model, the level set formulation of the energy functional $F_\alpha(c)$ in scale S_α is then expressed by

$$F_\alpha(c) = R_\alpha \left[\mu \int_{\Omega_0} |\nabla H_\phi| dxdy + \sum_{i=1}^{4} \xi_{i,c} \int_{\Omega_0} \left(d^i - \bar{d}_1^i\right)^2 H_\phi \, dxdy + \sum_{i=1}^{4} \xi_{i,c} \int_{\Omega_0} \left(d^i - \bar{d}_2^i\right)^2 (1 - H_\phi) dxdy\right] \tag{9}$$

where $\alpha < N$. After obtaining the candidate contours in scale S_α, we can extract candidate contours in scale $S_{\alpha-1}$ in the same way as scale S_α, such that we can interactively obtain the object contours in original resolution images, whereas the computational cost is greatly reduced.

By comparing (7) and (9), we can see that the level set formulation for both coarse scale and fine scale can be written in a uniform expression by defining $R_N(x, y) = 1$, i.e.,

$$F_\alpha(c) = R_\alpha \left[\mu \int_{\Omega_0} |\nabla H_\phi| dxdy + \sum_{i=1}^{4} \xi_{i,c} \int_{\Omega_0} \left(d^i - \bar{d}_1^i\right)^2 \times H_\phi \, dxdy + \sum_{i=1}^{4} \xi_{i,c} \int_{\Omega_0} \left(d^i - \bar{d}_2^i\right)^2 (1 - H_\phi) dxdy\right] \tag{10}$$

where $1 \leq \alpha \leq N$. Therefore, we can give a common numerical solution to both coarse- and fine-scale models based on the uniform level set functional.

IV. Numerical Solution

Here, we describe the numerical solution to the uniform level set functional. In order to minimize the uniform level set functional, we deduce the associated Euler–Lagrange equation for ϕ by introducing the artificial variable t to ϕ. We then obtain the following:

$$\frac{\partial \phi}{\partial t} = \delta(\phi) R_\alpha \left[\mu \mathrm{div}\left(\frac{\nabla \phi}{|\nabla \phi|}\right) - \sum_{i=1}^{4} \left(\xi_{i,c}\left(d^i - \bar{d}_1^i\right)^2 - \xi_{i,c}\left(d^i - \bar{d}_2^i\right)^2\right)\right] \tag{11}$$

where $\delta(\cdot)$ is the Dirac function.

To discretize (11), we introduce the following finite difference items of function ϕ:

$$\begin{aligned}
\triangle^x \phi_{x,y} &= \frac{\phi_{x+1,y} - \phi_{x-1,y}}{2} \\
\triangle^{xx} \phi_{x,y} &= \phi_{x+1,y} - 2\phi_{x,y} + \phi_{x-1,y} \\
\triangle^y \phi_{x,y} &= \frac{\phi_{x,y+1} - \phi_{x,y-1}}{2} \\
\triangle^{yy} \phi_{x,y} &= \phi_{x,y+1} - 2\phi_{x,y} + \phi_{x,y-1} \\
\triangle^{xy} \phi_{x,y} &= \triangle^y \phi_{x+1,y} - \triangle^y \phi_{x-1,y} 2.
\end{aligned}$$

The curvature item in (11) is approximated by the difference items as follows:

$$\mathrm{div}\left(\frac{\nabla \phi}{|\nabla \phi|}\right)_{x,y} = \frac{\triangle^{xx}\phi(\triangle^y\phi)^2 - 2\triangle^x\phi\triangle^y\phi\triangle^{xy}\phi + \triangle^{yy}\phi(\triangle^x\phi)^2}{\left[(\triangle^x\phi)^2 + (\triangle^y\phi)^2\right]^{3/2}}.$$

Due to the fact that the Dirac function concentrates at 0, it is approximated by the compactly supported regularized function defined as follows:

$$\delta_{\epsilon_1}(x) = \frac{1}{\pi} \cdot \frac{\epsilon_1}{\epsilon_1^2 + x^2}. \tag{12}$$

Then, the level set functional (11) can be solved by the following iterative computing scheme:

$$\phi_{x,y}^{n+1} = \phi_{x,y}^{n} + \triangle t \cdot R_\alpha \cdot \delta_\epsilon\left(\phi_{x,y}^{n}\right)\left[\mu\,\mathrm{div}\left(\frac{\nabla\phi}{|\nabla\phi|}\right)_{x,y} - \sum_{i=1}^{4}\left(\xi_{i,c}\left(d_{x,y}^{i}-\bar{d}_1^{i}\right)^2 - \xi_{i,c}\left(d_{x,y}^{i}-\bar{d}_2^{i}\right)^2\right)\right]. \quad (13)$$

Based on the aforementioned description, the principal steps for the N-level schemes of our method are listed as follows.

1) Create the multiscale images from scale S_1 to S_N by (6), and let $\alpha = N$.
2) If $\alpha < N$, map the candidate contour in scale $S_{\alpha+1}$ to S_α to obtain the initial curves γ_α; otherwise, set the initial curves γ_N in scale S_N.
3) If $n = 0$, initialize ϕ^n according to curve γ_α, and compute the contour position constraint R_α.
4) Use the narrow-band method [10] to compute ϕ^{n+1} by (14). Reinitialize ϕ^{n+1}. Then, check wether the solution is stationary. If not, $n = n + 1$, and repeat this step.
5) If $\alpha = \alpha - 1$, repeat steps 2, 3, and 4 until $\alpha < 1$.

The direct implementation of step 4 is computationally expensive. However, this problem can be solved by the narrow-band method (please refer to [10] for details) and the contour position constraint in our method. Note that the narrow-band method makes the level set evolve in a small region around the candidate contours.

V. Experimental Results

Here, extensive experiments are conducted to evaluate the performance of the proposed method. The test database is provided by the Equipment Advanced Research Project and contains 263 optical images from the WorldView satellite, the QuickBird satellite, and so on. Each test image contains at least one salient object whose resolution ranges from 0.5 to 1 m. The ground-truth contours of the salient objects are hand labeled by satellite image interpretators.

All methods were implemented in C++ on a personal computer with a Pentium IV 3.4-GHz central processing unit. We set the initial curves using a group of 60 × 60 squares, which are uniformly arranged with a 20-pixel interval between each other, and reinitialize the level set function every five evolution iterations using the Euclidean-distance-transform algorithm [11] for all implementations. In all experiments, the model parameters were set as follows: $\triangle t = 0.1$, $\epsilon_0 = 0.01$, $\epsilon_1 = 1$, and the curve length weight $\mu = 0.5$.

A. Accuracy Comparison

We compared the accuracy of the proposed method with the most recent multiscale method [8] and the tensor-feature-based method [6]. In the experiments, the scale levels of both multiscale methods were set to three, i.e., $N = 3$. In order to perform quantitative analysis, the success score used in [6] was adopted to measure the accuracy of extracted contours. Let Ω_{joint} be the regions both inside ground-truth and extracted contours, and let Ω_{union} be the regions inside the ground-truth or the extracted contours. The success score is defined as follows:

$$s = \frac{\text{number of pixels contained in } \Omega_{\text{joint}}}{\text{number of pixels contained in } \Omega_{\text{union}}}. \quad (14)$$

TABLE I
Accuracy of Different Methods on G_1 and G_2

	Proposed method		Method [6]		Method [8]	
	ASS	SDSS	ASS	SDSS	ASS	SDSS
G_1	0.936	0.053	0.912	0.087	0.901	0.116
G_2	0.907	0.061	0.891	0.095	0.474	0.211

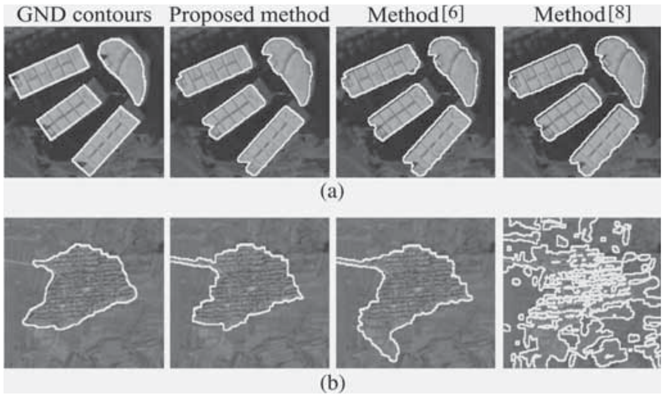

Fig. 2. Extracted contours of two test images using different methods. (a) Test image is 212 × 220 pixels and is taken from G_1. (b) Test image is 1266 × 1278 pixels and is taken from G_2.

Clearly, $0 \leq s \leq 1$. For the hand-labeled contours, the success score is 1.

Different methods were applied to extract contours from all test images. In order to get some insight on the experimental results, the test images were divided into groups G_1 and G_2. G_1 contains 127 images that present the salient intensity difference between objects and the background, whereas G_2 contains the remaining 136 images, which present the small intensity difference but the salient texture difference between objects and the background. We recorded the average and standard deviations of success scores for both groups (see Table I).

As for G_1, the average success scores of the methods in [6] and [8] were 0.912 and 0.901, respectively. An example of a good result is shown in Fig. 2(a). Our method achieved a better average success score of 0.936 and a smaller standard deviation of 0.053. One big reason for the good performance of our method is that the contour evolution space is constrained in the neighborhood of the candidate contours by the contour position constraint. Without the constraint, the average success score of our method reduced to 0.923 in the experiments. As for G_2, the average success scores of the method in [6] and our method were 0.891 and 0.907, respectively, whereas the average success score of the method in [8] was less than 0.5, [e.g., see Fig. 2(b)]. This is because the method in [8] mainly uses intensity features, whereas the intensity difference between objects and the background is small for G_2. In the experiments, we found that it is much easier to obtain accurate candidate contours in a coarse scale; therefore, the result of our method is also slightly better than that in [6].

In order to compare the noise robustness of the proposed method and the methods in [6] and [8], we performed experiments by adding 5%, 10%, and 15% Gaussian noise to the images in G_1 and G_2. The test results are shown in Table II. In Table II, we can see that, when adding 5%, 10%, and 15% noise, the performance of the methods in [6] and [8] decreased more rapidly than the proposed method. For example, when

TABLE II
ACCURACY OF DIFFERENT METHODS ON NOISY IMAGES

		Proposed method		Method [6]		Method [8]	
	Noise	ASS	SDSS	ASS	SDSS	ASS	SDSS
G_1	5%	0.930	0.062	0.902	0.098	0.884	0.151
	10%	0.919	0.074	0.857	0.113	0.810	0.189
	15%	0.908	0.082	0.814	0.196	0.708	0.217
G_2	5%	0.901	0.083	0.877	0.113	0.420	0.263
	10%	0.890	0.089	0.806	0.172	0.387	0.294
	15%	0.883	0.093	0.754	0.266	0.364	0.310

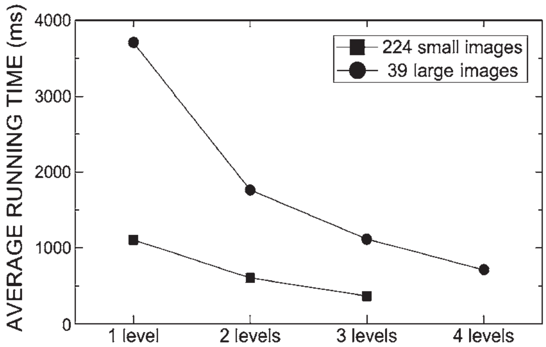

Fig. 3. ATPM of different scale levels of the proposed method for small and large images, respectively.

the images are heavily corrupted by adding up to 15% noise, the average success scores of the proposed method for G_1 and G_2 decreased to 0.028 and 0.024, whereas it decreased to 0.098 and 0.137 for the method in [6] and 0.193 and 0.11 for the method in [8]. In our opinion, the noise robustness of the proposed method is attributed to the contour position constraint and the noise removal scheme at the coarse scale by the average downsampling process.

B. Computational Efficiency Analysis

Here, we compare the running time of the proposed method with the ones in [6] and [8]. The scale levels of the method in [8] were set to three for all test images. As the images vary in size, the average running time (in millisecond) per million pixels (ATPM) was adopted to measure computational efficiency. Usually, the running time is not linearly increased as the image size increases; therefore, we compute the average running time separately for the 39 larger images (more than four million pixels) and the remaining 224 smaller images.

In our experiments, the ATPM of the methods in [6] and [8] are 1060 and 670 for small images, and 3910 and 3620 for large images, respectively. As for our method, we performed experiments from one to four scale levels on large images and from one to three scale levels on small images. The experimental results are shown in Fig. 3. The ATPM of our single-level scheme are 1130 for small images and 3790 for large images. The difference of computational efficiency between the competing methods and our single-level scheme is small. However, from two to four levels, the computational efficiency of our method greatly outperforms the competing methods. As shown in Fig. 3, compared with the single-level scheme, the three-level scheme reduced the running time by more than 50%. As for the larger images, the four-level scheme reduced more than 80% running time. Generally speaking, higher level

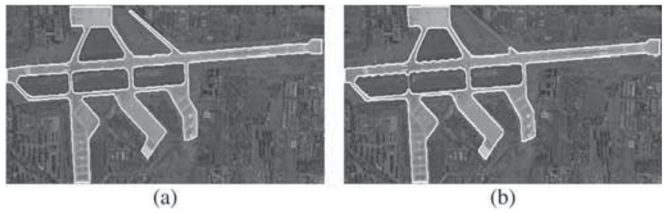

Fig. 4. Some parts of the contours lost when the scale levels of the proposed method exceed three. The size of the image is 4578×2348 pixels. (a) Contours of the one scale level. (b) Contours of four scale levels.

schemes reduce more running time than lower level schemes. However, parts of the contours may be lost when the scale levels exceed a certain number(see Fig. 4). According to the experiments, the optimum scale levels without priorities should be set to three.

VI. CONCLUSION

In this letter, we have presented a coarse-to-fine level set method to extract object contours for optical satellite images. An adaptive weighting approach is proposed to tune the weights of wavelet features, and a novel energy functional is introduced into the level set method to model the contour extraction problem. Based on the model, a coarse-to-fine scheme is developed to progressively extract contours. The experiments on a large satellite-image database demonstrate that the proposed method achieves encouraging performance on the running time and improves the accuracy of the extracted contours, particularly the contours obtained from noisy images. In the future, we plan to study how to automatically select the scale levels for the proposed method.

REFERENCES

[1] J. Elder, "The visual computation of bounding contours," Ph.D. dissertation, Dept. Elect. Eng., McGill Univ., Montreal, QC, Canada, 1995.
[2] T. F. Chan and L. A. Vese, "Active contours without edges," *IEEE Trans. Image Process.*, vol. 10, no. 2, pp. 266–277, Feb. 2001.
[3] N. Lin, W. Yu, and J. S. Duncan, "Combinative multi-scale level set framework for echocardiographic image segmentation," *Med. Image Anal.*, vol. 7, no. 4, pp. 529–537, Dec. 2003.
[4] S. Yongmin, S. Hong, and X. Ge, "SAR image segmentation based on level set with stationary global minimum," *IEEE Geosci. Remote Sens. Lett.*, vol. 5, no. 4, pp. 644–648, Oct. 2008.
[5] M. Silveira and S. Heleno, "Separation between water and land in SAR images using region-based level sets," *IEEE Geosci. Remote Sens. Lett.*, vol. 6, no. 3, pp. 471–475, Jul. 2009.
[6] R. de Luis-Garcıacute;a, R. Deriche, and C. Alberola-López, "Texture and color segmentation based on the combined use of the structure tensor and the image components," *Signal Process.*, vol. 88, no. 4, pp. 776–795, Apr. 2008.
[7] W. Bin, G. Xinbo, T. Dacheng, and L. Xuelong, "A unified tensor level set for image segmentation," *IEEE Trans. Syst., Man, Cybern. B, Cybern.*, vol. 40, no. 3, pp. 857–867, Jun. 2010.
[8] Y. N. Law, H. K. Lee, and A. M. Yip, "A multiresolution stochastic level set method for Mumford–Shah image segmentation," *IEEE Trans. Image Process.*, vol. 17, no. 12, pp. 2289–2300, Dec. 2008.
[9] J. L. Starck, J. Fadili, and F. Murtagh, "The undecimated wavelet decomposition and its reconstruction," *IEEE Trans. Image Process.*, vol. 16, no. 2, pp. 297–309, Feb. 2007.
[10] S. Yui, K. Hara, H. Zha, and T. Hasegawa, "Acceleration of narrow band method and its application to topology-adaptive 3D geometrical modeling," *Syst. Comput. Jpn.*, vol. 37, no. 11, pp. 68–78, Oct. 2006.
[11] Y. Lucet, "New sequential exact Euclidean distance transform algorithms based on convex analysis," *Image Vis. Comput.*, vol. 27, no. 1/2, pp. 37–44, Jan. 2009.